Low-Voltage Ride-Through Based on Neuro-Fuzzy for Grid-Connected Photovoltaic System

N. Jaalam[1,2], L. V. Tan[1], N. H. Ramly[1], L. N. Muhammad[1], N. L. Ramli[1], and N. L. Ismail[3]
[1] Faculty of Electrical & Electronics Engineering Technology, University of Malaysia Pahang, 26600 Pekan, Malaysia
[2] UMPEDAC, University of Malaya, 59100 Kuala Lumpur, Malaysia
[3] Faculty of Engineering, National Defence University of Malaysia, Kem Sungai Besi, 57000 Kuala Lumpur, Malaysia
Email: {zila; hafeizza; lailatul; noorlina}@ump.edu.my; liven9595@gmail.com; norlaili@upnm.edu.my

***Abstract*—The increasing capacity of grid-connected photovoltaic (PV) over electrical power system might lead to voltage sags which affected the consumers and industries. To improve this situation, a simple control strategy of reactive power control using neuro-fuzzy is proposed in this paper to enable voltage regulation in a single-stage grid-connected PV system. An Artificial Neural Network (ANN) model is trained until a satisfactory result is obtained. After that, the trained neural network is combined with fuzzy logic. During the abnormal condition, the reactive current is controlled to inject reactive power for grid support and voltage recovery purpose. The dynamic behaviour of the system will be analyzed under a three-phase fault condition via MATLAB/Simulink. The simulation result shows that the proposed control strategy using neuro-fuzzy controller is effective in compensating desired reactive power during such faults. The voltage profile of the system has shown at least 9% of increment in all case studies. A swift recovery on the voltage can be achieved as well since the voltage returns to steady-state immediately when the fault is cleared.**

***Index Terms*—Low-voltage ride-through, grid-connected photovoltaic, neuro-fuzzy**

I. Introduction

In today's world, the increment in dependency on electricity usage might cause a problem as fossil fuels reserve diminish. It takes millions of years to form fossil fuels and they cannot be replaced once depleted. In this case, solar power is found to be an attractive approach to offset human dependence on electricity that is generated from fossil fuels. Fig. 1 shows that solar is the most popular Renewable Energy Sources (RES) with 55% of installation compared to other renewable energy [1]. According to the Global Status Report, a total of 402 GW PV systems has been installed worldwide until 2017 [2].

Distributed Generation (DG) is a small scale energy resources that are located close to the end-users where PV is one of the most common types of DG technologies that provide high power reliability and low-cost electricity.

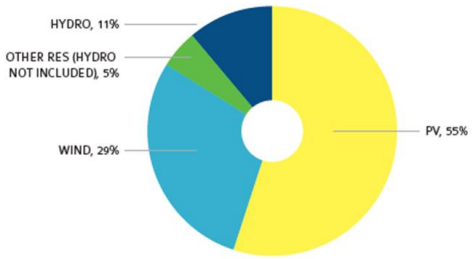

Fig. 1. PV share in the total renewable energy sources installation [1].

However, there are some disadvantages when PV-based DG (PVDG) is implemented. Reverse power flow might happen when the penetration level of PVDG is high which in turn might affect the protection scheme in the system. Besides, voltage fluctuations might occur due to the PV uncertainty sources that will increase losses and shorten the lifespan of the equipment. It will also lead to system instability and power outage. Voltage instability is known to be the most problematic electrical disturbances with 80% of power quality incidents is caused by voltage sag [3]-[5]. A single disruption in electricity supply might cause these industries to suffer huge losses up to millions of dollars [6].

Because of these shortcomings, the grid-connected PV system is expected to provide a full range of service during fault occurrence. During such fault, even the voltage decreased to its lowest point, the DG should not be disconnected and must continuously support the grid by injecting a reactive power. This service helps in stabilizing the power grid and it is known as Low-Voltage ride-through (LVRT) function. By implementing this, flickers and many other power quality problems that may lead to a fatal breakdown can be avoided [7], [8].

The LVRT implementation in PV-based system is still considered new if compared to wind power system [9], [10]. Some of the developed countries which already implemented the LVRT with their own standard are Germany, Italy, and Japan, to name a few [11]. Fig. 2 demonstrates the LVRT requirements defined by Germany which has three main divisions divided by Borderline 1 and 2 [12]. The DG must continue its normal operation if the voltage decrement is upper than Borderline 1 and 2 for the given time range. Even if the voltage decrease for more than 70% from its nominal value, the DG shall continue its operation as long as it

Manuscript received November 28, 2019; revised January 12, 2020; accepted March 6, 2020.
Corresponding author: N. Jaalam (email: zila@ump.edu.my).
This work has been supported by the University of Malaysia Pahang (Grant number: RDU1703282) and the Ministry of Higher Education of Malaysia.

doi: 10.18178/ijeetc.9.4.260-267

iswithin 150 milliseconds (ms). This is the time where reactive power injection is needed. Nonetheless, if the voltage decrement below Borderline 2, the DG must be disconnected immediately.

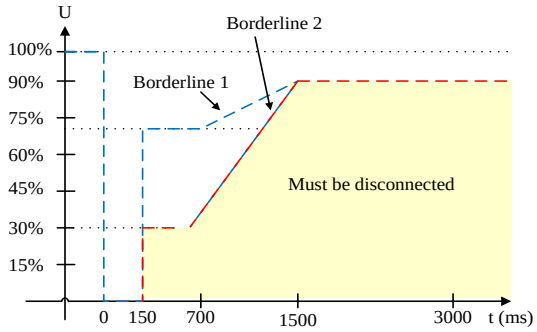

Fig. 2. LVRT requirements defined by Germany grid code [12].

Numerous effort has been performed to implement LVRT in power generation plant [13]-[17]. Yang *et al*. presents a control approach for active and reactive power using a conventional PI controller for a 500 kW PV system with LVRT [18]. It is a double-stage system with MPPT. The MPPT is switched off when the voltage sag is detected. The effectiveness of the proposed system was tested with three-phase symmetrical fault only. A PI method is also used for 40 kW PV system in [19]. A result obtained from MATLAB/Simulink has confirmed the effectiveness of the scheme under varying irradiance only, but the efficiency under other severe disturbances has not yet been tested. In addition, the PI controller is also known for its drawback in which tuning the correct value would take a very long time especially under severe grid disturbances. Thus, the desired control performance of the PI controller cannot be assured.

Therefore, an approach to enhance the LVRT capability using neuro-fuzzy scheme is proposed. An analysis of 1 MW single-stage grid-connected PV system will be provided which will consider the dynamic response of the reactive power of the PVDG inverter. All assessments and verifications will be carried out in MATLAB/ Simulink environment. This paper is organized as follows: Section II presents a basic control strategy of the PVDG while Section III explained the control strategy of the neuro-fuzzy scheme. The performance of the PVDG with LVRT capability under three-phase fault conditions will be discussed in Section IV and finally, Section V will address the final conclusion of this research paper.

II. Basic Control Structure of a Single-Stage Grid-Connected PV System

A basic structure of a single-stage grid-connected PV system is shown in Fig. 3. The PV array is connected to the DC-AC inverter through a DC-link capacitor, i.e. C_{DC} that can be calculated by

$$C_{DC} = \frac{P}{2\omega V_{DC,nominal} V_{ripple}} \quad (1)$$

where ω is the AC frequency and V_{ripple} is the maximum allowed voltage ripple [20].

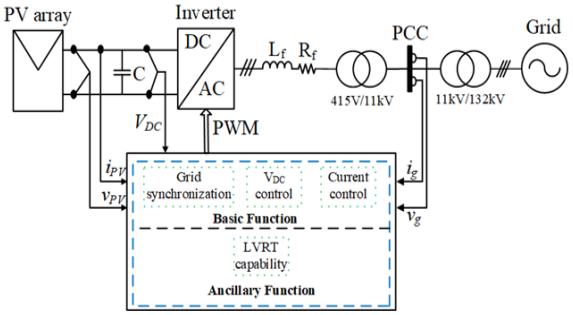

Fig. 3. Single-stage grid-connected PV system.

The inverter plays a vital role in this configuration as it is used to convert DC power generated from the PV array to an AC power and allows the PV array to be integrated into the grid. This can be done using a basic control function of the inverter which consists of DC-link voltage (V_{DC}) control, internal current control loop, and grid synchronization function as illustrates in Fig. 4. The function of V_{DC} control is to normalize the voltage where C_{DC} is important to minimize V_{DC} ripple [21]. Meanwhile, the internal current loop is essential to control the instantaneous grid current whereas the grid synchronization function is to track the frequency and phase angle of the grid for the successful integration. The grid synchronization function can be realized with the help of a Phase-Locked Loop (PLL).

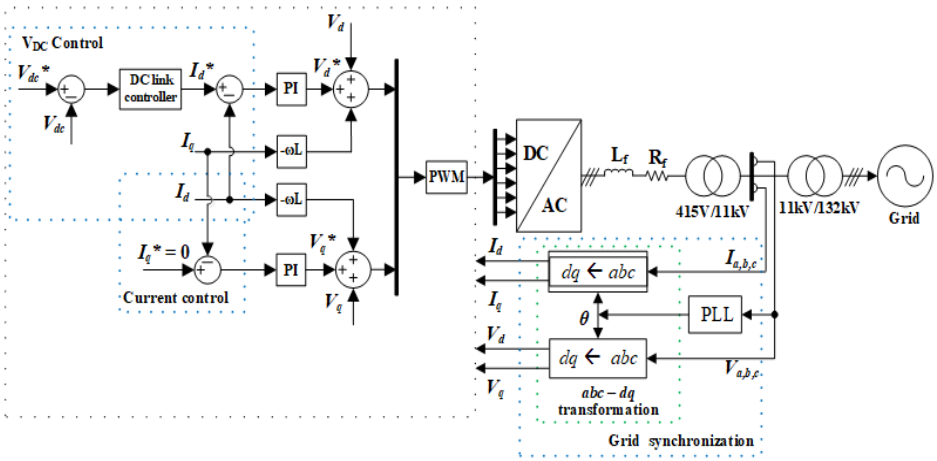

Fig. 4. Basic control function of grid-connected PV system.

For the VSI modeling, the three-phase voltage can be adopted as:

$$\begin{cases} V_a = L\dfrac{dI_a}{dt} + Ri_a + V_{ga} \\ V_b = L\dfrac{dI_b}{dt} + Ri_b + V_{gb} \\ V_c = L\dfrac{dI_c}{dt} + Ri_c + V_{gc} \end{cases} \quad (2)$$

where the V_a, V_b, and V_c are the inverter voltage; i_a, i_b, and i_c are the inverter current; and V_{ga}, V_{gb}, and V_{gc} are the grid voltage respectively.

Then, the three-phase quantities of grid voltage were transformed into two-phase quantities (d, q) using Park's Transformation. After the transformation, the mathematical model of the inverter in the dq synchronous reference frame can be obtained from the equations as follows:

$$V_d = L\frac{dI_d}{dt} + Ri_d + V_{gd} \quad (3)$$

$$V_q = L\frac{dI_q}{dt} + Ri_q + V_{gq} \quad (4)$$

where I_d, V_{gd}, I_q, and V_{qd} represent the d- and q-axis current and voltage at grid side in dq synchronous frame.

Subsequently, the equations for active (P) and reactive (Q) power of the inverter can be calculated as

$$P = \frac{3}{2}\left(V_{gd}I_d + V_{qd}I_q\right) \quad (5)$$

$$Q = \frac{3}{2}\left(-V_{gd}I_q + V_{qd}I_d\right) \quad (6)$$

However, when a voltage space vector is on the d-axis resulted in V_{qd} is equal to zero, equation (5) and (6) can be simplified to:

$$P = \frac{3}{2}\left(V_{gd}I_d\right) \quad (7)$$

$$Q = \frac{3}{2}\left(-V_{gd}I_q\right) \quad (8)$$

TABLE I: PARAMETERS OF SUN POWER 305 PV MODULE AT STC

Parameter at STC	Value
Maximum power, P_{mp}	305 W
Open circuit voltage, V_{oc}	64.2 V
Voltage at maximum power, V_{mp}	54.7 V
Short circuit current, I_{sc}	5.96 A
Current at maximum power, I_{mp}	5.58 A
Number of solar cells	96
Temperature coefficient P_{mp}	-0.38 %/°C
Temperature coefficient V_{oc}	-176.6 mV/°C
Temperature coefficient I_{sc}	3.5 mA/°C
Maximum system voltage	1000 V

In order to accomplish the proposed single-stage grid-connected PV system, the PV module needs to be connected in parallel and series configuration to increase its current and voltage accordingly to achieve the rated power of 1 MW. In this study, a configuration of 15 series module and 220 parallel strings is chosen to form the PV array. The parameters of the SunPower 305 PV module are listed in Table I. Meanwhile, the system parameters used in this study are listed in Table II.

TABLE II: SYSTEM PARAMETERS USED IN THE STUDY

Parameter	Value
Rated power, P_{rated}	1 MW
Grid voltage (grid side)	11 kV
Grid voltage (PV side), V_g	415 V_{rms}
Voltage at maximum power, V_{mp}	930 V
Output filter, L_f	0.05 mH
Switching frequency, f_{sw}	10 kHz
Grid frequency, f_g	50 Hz

III. LVRT CONTROL STRATEGY WITH REACTIVE POWER INJECTION

The LVRT requirement stipulates that the PV system must stay connected to the grid under certain weak grid condition. In the meantime, the reactive current injection (RPI) should be supplied to the system to improve the voltage profile. For the successful implementation of the RPI, the system must be able to detect the faulty mode operation first as described in Fig. 5. The grid voltage, V_g will be continuously measured whether it is still in a specified range or not. If it exceeds the range, an appropriate action through RPI will take place to prevent voltage disturbance by injecting or absorbing the supplied reactive power.

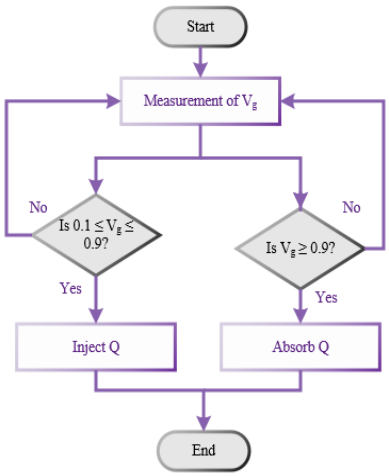

Fig. 5. Flow chart for fault detection method.

A. RPI Enhancement Using Neuro-fuzzy Scheme

The RPI can be enhanced using neuro-fuzzy scheme. As the name suggests, this technique combines ANN and fuzzy logic into a system. During tuning of fuzzy controller, the choice of membership functions and fuzzy rules can affect the quality of the controller drastically. Although fuzzy logic might seem easier to design based on knowledge and experience, the actual development process to design and tune the membership functions is very time-consuming. Neuro-fuzzy uses ANN learning techniques to solve this problem in which the learning

techniques of ANN can automate the tuning process of fuzzy. This substantially reduces the time of the conventional trial and error method while improving performance.

B. ANN Model

Validation, training and testing data sets for the ANN are generated using PI controller from the system. The data sets are inserted and exported using *nntool* of MATLAB. The network is then created and configured by selecting input data, target data, data sets percentage as well as the number of the hidden neurons. After that, the network is trained to fit the inputs and targets. Due to different sampling and initial conditions, different results will be generated by multiple training. The network is validated by checking the validation error during the training process. Finally, the ANN model is tested in the system before the network is being used.

Fig. 6 shows the feed-forward neural network architecture which is made up of one input, output and hidden layer. In this case, the input layer represents the grid voltage, V_g while the output layer represents the reactive current, I_q. The number of neurons in the hidden layer is variable based on the best results. Since more parameters can be considered with larger hidden neurons number, the flexibility of the network increase. After many trials, the optimum neuron number is two as it gives better performance with relatively low error. Linear transfer function (purelin) is chosen for the output layer whereas symmetric sigmoid transfer function (tansig) is chosen for the hidden layer. The ANN model is trained using Levenberg Marquardt back propagation. It is important to monitor the validation error during the training process to prevent overfitting problem.

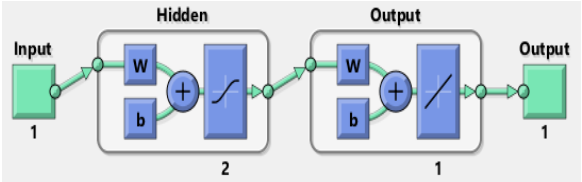

Fig. 6. Feed forward neural network in Simulink.

C. Neuro-Fuzzy Model

The trained neural network is then combined with fuzzy logic where the output of ANN will be the input for fuzzy logic. The linguistic variables (reactive current and grid voltage) and their respective numerical range are defined. The grid voltage is the input while the reactive current is the output. For the fuzzy logic controller, the fuzzy sets are designed using Gaussian combination membership function (gauss2mf) and Mamdani style inference as shown in Fig. 7 and 8. Fuzzy rules are constructed based on experience and the expected performance. In this study, the number of rules is 9 as shown in Table III. The fuzzy sets, as well as fuzzy rules and its evaluations, are encoded to perform fuzzy inference into the fuzzy system. The linguistic variables that representing grid voltage and reactive current are Positive Very Large (PVL), positive large (PL), Positive Medium (PM), Positive Small (PS), Zero (Z), Negative Small (NS), Negative Medium (NM), Negative Large (NL) and Negative Very Large (NVL) respectively.

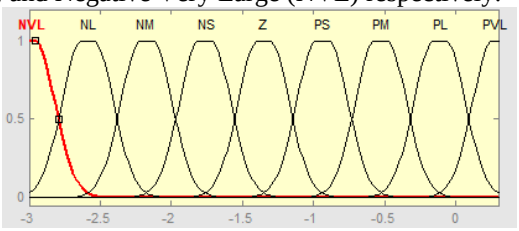

Fig. 7. Fuzzy set for grid voltage.

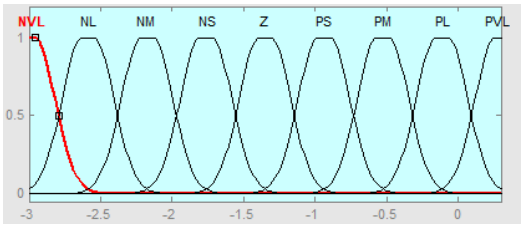

Fig. 8. Fuzzy set for reactive current.

TABLE III: RULE BASE FOR THE NEURO-FUZZY CONTROLLER

Input	NVL	NL	NM	NS	Z	PS	PM	PL	PVL
Output	NVL	NL	NM	NS	Z	PS	PM	PL	PVL

IV. SIMULATION RESULT

This section presents the results of ANN performance and LVRT enhancement with RPI using the proposed neuro-fuzzy controller with 10%, 20% and 30% voltage decrement. The power vs. voltage (*P-V*) and current vs. voltage (*I-V*) curve of the PV array is also presented.

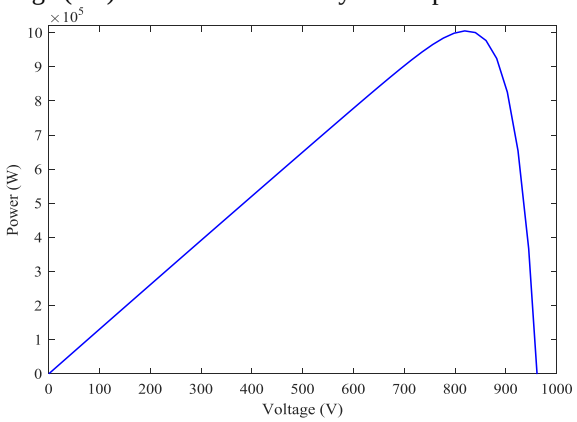

Fig. 9. P-V curve of the PV array.

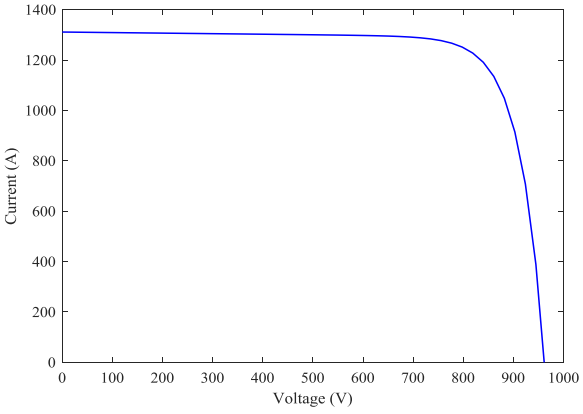

Fig. 10. I-V curve of the PV array.

A. P-V and I-V Curve of 1 MW PV Array

Fig. 9 and Fig. 10 illustrate the *P-V* curve and *I-V* curve of the PV array. With 15 series-connected modules per string and 220 parallel string, the system generates 1.0065 MW with I_{sc}= 1311.2 A and V_{oc} = 963 V.

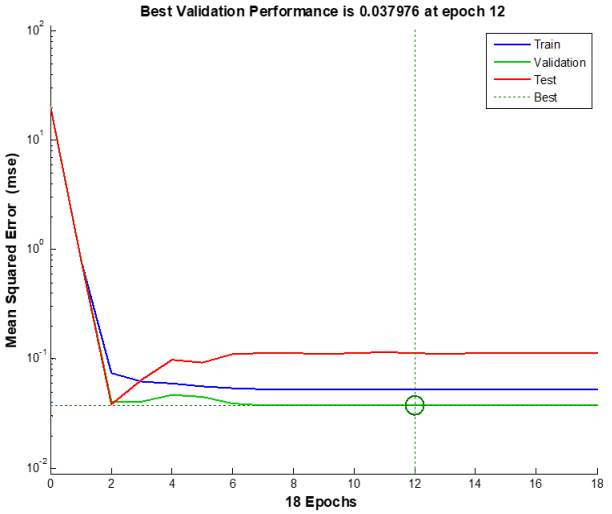

Fig. 11. Performance of ANN with 10% voltage decrement.

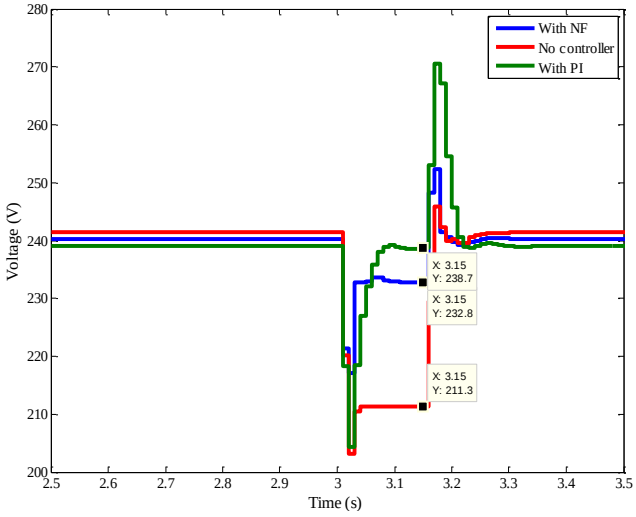

Fig. 12. Inverter voltage with neuro-fuzzy, PI and without controller.

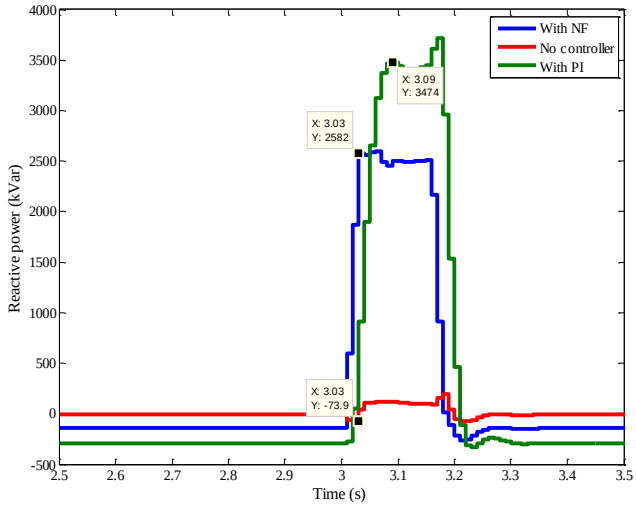

Fig. 13. Reactive power with neuro-fuzzy, PI and without controller.

B. Case Study with 10% Voltage Decrement

For a 10% voltage decrement, Epoch 12 gives the best validation performance with an MSE value of 0.037976 as shown in Fig. 11. The performance plot indicates that no major problems have been found in the training. No overfitting has occurred since the validation and test curves are almost similar with no crossing over. The result is acceptable since the training and testing results are quite alike and do not differ much from each other.

The fault resistance is set to 15 Ω with 1000 W/m^2 irradiance in this case. Fig. 12 and 13 show the inverter voltage and reactive power with neuro-fuzzy (NF), PI controller as well as without controller. When the three-phase fault occurred at 3.0 s, the voltage experiences a significant drop. Without a controller, the voltage decreased to 211.3 V as the RPI is zero. Meanwhile, the system with NF shows an improvement where the voltage increased to 232.8 V, an increment by 9%. This can be done by controlling I_q to compensate the reactive power. As a result, 2582 kVar is injected into the system to improve the voltage profile. When the fault is cleared at 3.15 s, both voltage and reactive power return to its steady-state immediately.

On the other hand, the system with PI also shows an improvement where the voltage increased to 238.7 V, an increment by 11% to compensate the voltage drop. As a result, 3474 kVar is injected into the system to improve the voltage profile. In terms of the voltage profile improvement, PI controller performs slightly better than NF controller. However, PI controller tends to have a slower recovery to steady-state compared to the system with NF controller.

C. Case Study with 20% Voltage Decrement

Fig. 14 shows Epoch 9 gives the best validation performance with an MSE value of 0.0080356 for a 20% voltage decrement. The performance plot indicates that no major problems have been found in the training. No overfitting has occurred since the test curve did not increase substantially before the increment of the validation curve. The result is acceptable since the training and testing results are almost similar and do not differ much from each other.

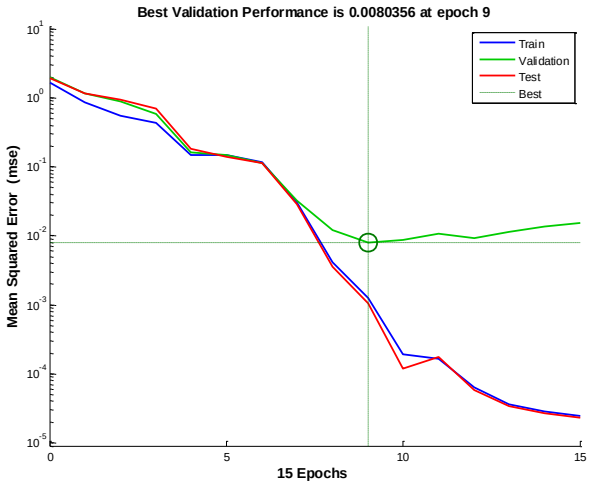

Fig. 14. Performance of ANN with 20% voltage decrement.

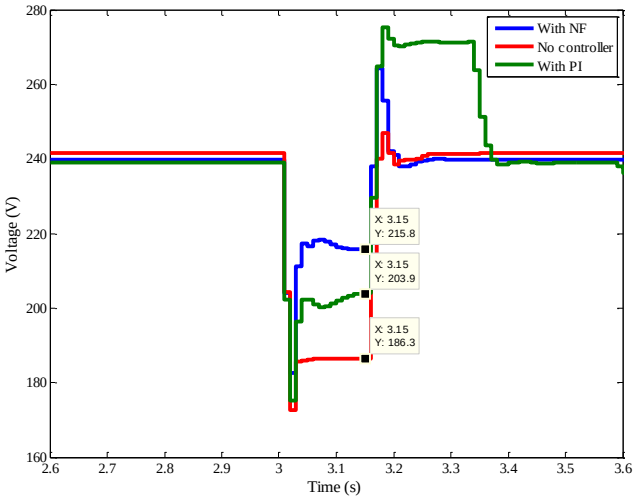

Fig. 15. Inverter voltage with neuro-fuzzy, PI and without controller.

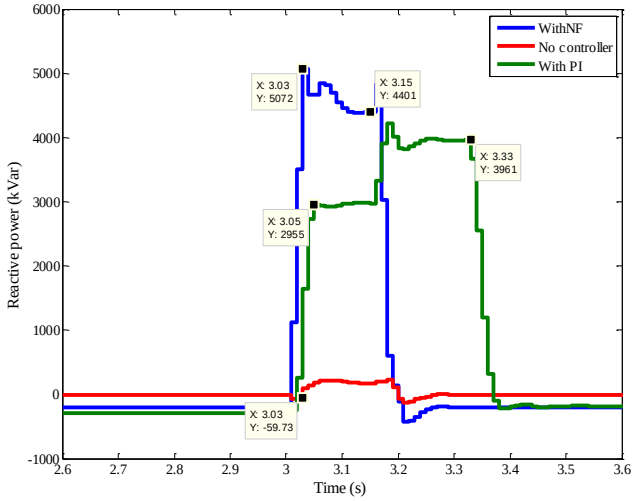

Fig. 16. Reactive power with neuro-fuzzy, PI and without controller.

In this case, the fault resistance is set to 7.5 Ω and the irradiance is maintained at 1000 W/m^2. Again, when the three-phase fault occurred at 3.0 s, the voltage experiences a significant decrement as shown in Fig. 15. Without a controller, the voltage decreased to 186.3 V as there is no injection of reactive power. On the other hand, the voltage improved to 215.8 V, an increment by 12% since the reactive power is injected into the system with NF controller as shown in Fig. 16. When the fault is cleared at 3.15 s, both voltage and reactive power return to its steady-state immediately.

Meanwhile, the system with PI also shows an improvement where the voltage increased to 203.9 V, an increment by 7% as the reactive power is injected into the system. In terms of the voltage profile improvement, NF controller performs better than PI controller. Besides, the system with NF controller shows rapid recovery to steady-state compared to PI controller. It can be observed that PI controller tends to return to steady-state at a slower rate as illustrated in Fig. 15 and Fig. 16.

D. Case Study with 30% Voltage Decrement

For a 30% voltage decrement, Epoch 241 gives the best validation performance with an MSE value of 7.471×10^{-5} as shown in Fig. 17. The performance plot indicates that no major problems have been found in the training. No overfitting has occurred since the validation and test curves are almost similar with no crossing over. The result is acceptable since the training and testing results are quite alike and do not differ much from each other.

The fault resistance is set to 5 Ω with 1000 W/m^2 irradiance in this case. Again, when the three-phase fault occurred at 3.0 s, the voltage experiences a significant decrement as shown in Fig. 18. Without a controller, the voltage decreased to 164.6 V as the RPI is zero. Meanwhile, the voltage improved to 195.2 V, an increment by 13% since the reactive power is injected into the system with NF controller as shown in Fig. 19. When the fault is cleared at 3.15 s, both voltage and reactive power return to its steady-state immediately.

On the other hand, the system with PI also shows an improvement where the voltage increased to 178.6 V, an increment by 6% as the reactive power is injected into the system. In terms of the voltage profile improvement, NF controller performs better than PI controller. Besides, the system with NF controller shows speedy recovery to steady-state compared to PI controller. It can be seen that PI controller tends to return to steady-state at a slower rate as illustrated in Fig. 18 and Fig. 19.

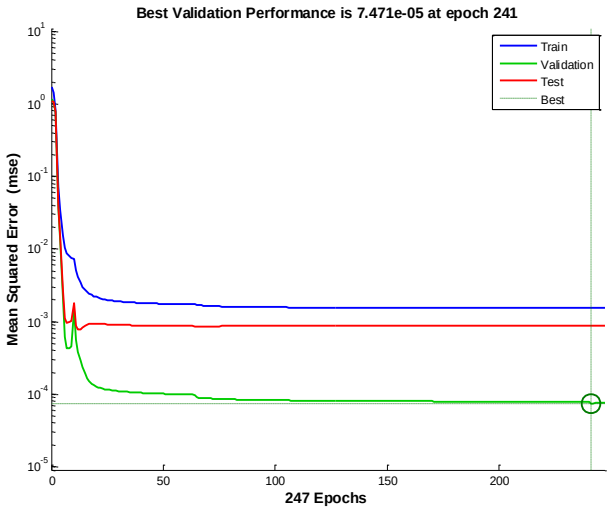

Fig. 17. Performance of ANN with 30% voltage decrement.

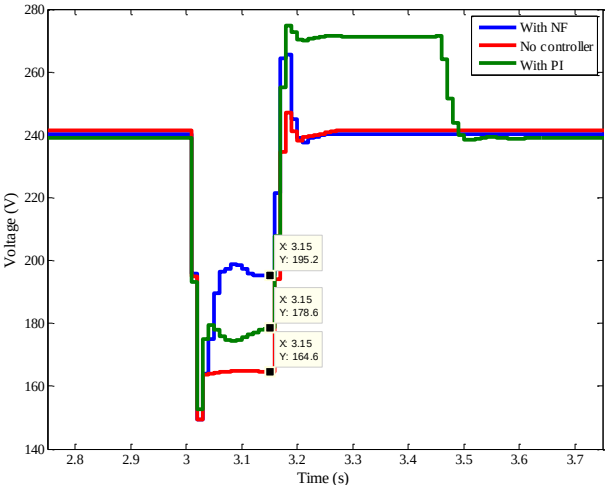

Fig. 18. Inverter voltage with neuro-fuzzy, PI and without controller.

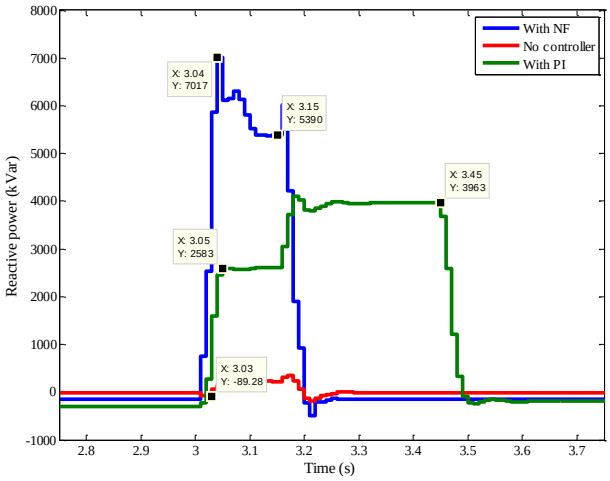

Fig. 19. Reactive power with neuro-fuzzy, PI and without controller.

V. Conclusion

A simple control strategy based on neuro-fuzzy controller has been proposed to provide LVRT capability for the single-stage grid-connected PV system. The system was compared with the conventional PI controller and the system without a controller to show its effectiveness. The results obtained from MATLAB/Simulink show that the proposed control strategy using neuro-fuzzy controller is effective in compensating reactive power into the grid to improve the voltage profile and reduced the time consumed for tuning the conventional PI controller. It was proven that neuro-fuzzy gives better performance in terms of voltage profile improvement. A swift recovery can be achieved as neuro-fuzzy returns to steady-state immediately compare to PI when the fault is cleared. Under 10%, 20% and 30% voltage decrement, the controller manages to control the reactive current so that the voltage can be improved by at least 9%. Thus, the power grid can maintain its stability and reliability.

Conflict of Interest

The authors declare no conflict of interest.

Author Contributions

N. Jaalam and L. V. Tan conducted the research, development of PV modelling and neuro-fuzzy; N. L. Ismail and L. N. Muhammad analyzed the data; N. Jaalam and L. V. Tan validated the results, wrote the paper with the cooperation of N. H. Ramly and N. L. Ramli that contributed on paper/figure editing; all authors had approved the final version.

References

[1] G. Masson and I. Kaizuka, Trends 2018 in Photovoltaic Applications - Survey Report of Selected IEA Countries between 1992 and 2017. IEA International Energy Agency, 2018.

[2] REN21, Renewables 2018 - Global Status Report, REN21 Secretariate. REN21 Secretariat, 2018.

[3] A. Honrubia-Escribano, E. Gómez-Lázaro, A. Molina-Garcia, and S. Martín-Martínez, "Load influence on the response of AC-Contactors under power quality disturbances," *Int. J. Electr. Power Energy Syst.*, vol. 63, pp. 846–854, 2014.

[4] F. H. Gandoman, A. Ahmadi, A. M. Sharaf, *et al.*, "Review of FACTS technologies and applications for power quality in smart grids with renewable energy systems," *Renew. Sustain. Energy Rev.*, vol. 82, pp. 502–514, 2018.

[5] P. Thakur and A. K. Singh, "Unbalance voltage sag fault-type characterization algorithm for recorded waveform," *IEEE Trans. Power Deliv.*, vol. 28, no. 2, pp. 1007–1014, 2013.

[6] M. F. Faisal, *Voltage Sag Solutions for Industrial Customers*, Tenaga Nasional Berhad, 2007.

[7] J. Dirksen, "Low voltage ride-through," *Dewi Magazine*, no. 43, pp. 56–60, 2013.

[8] M. S. El Moursi, W. Xiao, and J. L. Kirtley, "Fault ride through capability for grid interfacing large scale PV power plants," *IET Gener. Transm. Distrib.*, vol. 7, no. 9, pp. 1027–1036, 2013.

[9] J. E. G. Carrasco, J. M. Tena, D. Ugena, J. Alonso-Martinez, D. Santos-Martin, and S. Arnaltes, "Testing low voltage ride through capabilities of solar inverters," *Electr. Power Syst. Res.*, vol. 96, pp. 111–118, 2013.

[10] K. Kawabe and K. Tanaka, "Impact of dynamic behavior of photovoltaic power generation systems on short-term voltage stability," *IEEE Trans. Power Syst.*, vol. 30, no. 6, pp. 3416–3424, 2015.

[11] N. Jaalam, N. A. Rahim, A. H. A. Bakar, and B. M. Eid, "Strategy to enhance the low-voltage ride-through in photovoltaic system during multi-mode transition," *Sol. Energy*, vol. 153, pp. 744–754, 2017.

[12] A. Marinopoulos, F. Papandrea, M. Reza, S. Norrga, and F. Spertino, "Grid integration aspects of large solar PV installations: LVRT capability and reactive power/voltage support requirements," in *Proc. IEEE Trondheim PowerTech*, 2011, pp. 1–8.

[13] Y. Bae, T. Vu, and R. Kim, "Implemental control strategy for grid stabilization of grid-connected PV system based on german grid code in symmetrical low-to-medium voltage network," *IEEE Trans. Energy Convers.*, vol. 28, no. 3, pp. 619–631, 2013.

[14] M. Castilla, J. Miret, J. L. Sosa, J. Matas, and L. Garcá de Vicuna, "Grid-fault control scheme for three-phase photovoltaic inverters with adjustable power quality characteristics," *IEEE Trans. POWER Electron.*, vol. 25, no. 12, pp. 2930–2940, 2010.

[15] X. Guo, X. Zhang, B. Wang, W. Wu, and J. M. Guerrero, "Asymmetrical grid fault ride-through strategy of three-phase grid-connected inverter considering network impedance impact in low-voltage grid," *IEEE Trans. Power Electron.*, vol. 29, no. 3, pp. 1064–1068, 2014.

[16] J. Roldán-Pérez, A. García-Cerrada, J. L. Zamora-Macho, and M. Ochoa-Giménez, "Helping all generations of photo-voltaic inverters ride-through voltage sags," *IET Power Electron.*, vol. 7, no. 10, pp. 2555–2563, 2014.

[17] C. T. Lee, C. W. Hsu, and P. T. Cheng, "A low-voltage ride-through technique for grid-connected converters of distributed energy resources," *IEEE Trans. Ind. Appl.*, vol. 47, no. 4, pp. 1821–1832, 2011.

[18] F. Yang, L. Yang, and X. Ma, "An advanced control strategy of PV system for low-voltage ride-through capability enhancement," *Sol. Energy*, vol. 109, pp. 24–35, 2014.

[19] M. M. Hasaneen, M. A. L. Badr, and A. M. Atallah, "Control of active/reactive power and low-voltage ride through for 40 kW three-phase grid-connected single-stage PV system," *CIRED - Open Access Proc. J.*, vol. 2017, no. 1, pp. 1655–1659, 2017.

[20] K. Punitha, D. Devaraj, and S. Sakthivel, "Development and analysis of adaptive fuzzy controllers for photovoltaic system under varying atmospheric and partial shading condition," *Appl. Soft Comput. J.*, vol. 13, no. 11, pp. 4320–4332, 2013.

[21] B. Matic-Cuka and M. Kezunovic, "Islanding detection for inverter-based distributed generation using support vector machine method," *IEEE Trans. Smart Grid*, vol. 5, no. 6, pp. 2676–2686, 2014.

N. Jaalam received the bachelor's degree in electrical engineering (electronics) from University of Malaysia Pahang, Malaysia, in 2006, and M.Sc. in electrical power from Newcastle University, United Kingdom, in 2008. She is currently pursuing her Ph.D. degree in electrical engineering at University of Malaya, Kuala Lumpur, Malaysia. Her research field includes power electronics, renewable energy, artificial intelligence and energy management.

L. V. Tan received the B.Eng. (Hons.) degree in electrical engineering (power system) from University of Malaysia Pahang, Pekan, Malaysia, in 2019. She is currently working toward the M.Sc. degree in electrical engineering at University of Malaysia Pahang, Pekan, Malaysia. Her research interests include photovoltaic system, renewable energy, reactive power control, artificial intelligence and power electronics.

N. H. Ramly received the first degree in electrical engineering (electronics) from University of Malaysia Pahang, Malaysia, in 2006, and M.Sc. in electrical engineering (power) from University of Technology Malaysia, Skudai, Malaysia, in 2010. Her research field is in energy and power system study.

L. N. Muhammad received the diploma in electronics engineering and B.Eng. (Hons.) in electrical engineering (electronics) from University of Technology MARA, Shah Alam, Malaysia, in 2003 and 2007 respectively. Then, she graduated M.Sc. in electrical power engineering from University of Technology Malaysia, Skudai, Malaysia, in 2009. Currently, she is working as a lecturer at University of Malaysia Pahang. Her research field is power electronics, renewable energy and lightning protection system.

N. L. Ramli received the first degree in electrical engineering (electronics) from University of Malaysia Pahang, Malaysia, in 2006, and M.Sc. in power electronics and drives from Nottingham University, United Kingdom, in 2008. Currently, she is lecturer at University of Malaysia Pahang. Her research field is renewable energy and energy harvesting.

N. L. Ismail received the first degree in electrical engineering (electronics) from University of Malaysia Pahang, Malaysia, in 2006, and M.Sc. in electrical engineering from Nottingham University, United Kingdom, in 2008. Currently, she is pursuing her Ph.D. degree in electrical engineering at University of Technology MARA, Shah Alam, Malaysia. Her research field is power system study, renewable energy and artificial intelligence algorithm.